

DOI: 10.1002/adfm.((please insert DOI))

Defect engineering in oxide heterostructures by enhanced oxygen surface exchange

By *M. Huijben, G. Koster, * M.K. Kruize, S. Wenderich, J. Verbeeck, S. Bals, E. Slooten, B. Shi, H.J.A. Molegraaf, J.E. Kleibeuker, S. Van Aert, J.B. Goedkoop, A. Brinkman, D.H.A. Blank, M.S. Golden, G. Van Tendeloo, H. Hilgenkamp, and G. Rijnders*

[*] Dr. M. Huijben, Dr. G. Koster, M.K. Kruize, S. Wenderich, Dr. H.J.A. Molegraaf, Dr. J.E. Kleibeuker, Prof. A. Brinkman, Prof. D.H.A. Blank, Prof. H. Hilgenkamp, Prof. G. Rijnders
Faculty of Science and Technology and MESA+ Institute for Nanotechnology
University of Twente
7500 AE, Enschede, The Netherlands
E-mail: g.koster@utwente.nl
Dr. J. Verbeeck, Dr. S. Bals, Dr. S. van Aert, Prof. G. van Tendeloo
Electron Microscopy for Materials Science (EMAT)
University of Antwerp
2020 Antwerp, Belgium
E. Slooten, B. Shi, Dr. J.B. Goedkoop, Prof. M.S. Golden
Van der Waals-Zeeman Institute
University of Amsterdam
1090 GL, Amsterdam, The Netherlands

Keywords: defect engineering, oxide heterostructure, interface, electron gas, mobility

The synthesis of materials with well-controlled composition and structure improves our understanding of their intrinsic electrical transport properties. Recent developments in atomically controlled growth have been shown to be crucial in enabling the study of new physical phenomena in epitaxial oxide heterostructures. Nevertheless, these phenomena can be influenced by the presence of defects that act as extrinsic sources of both doping and impurity scattering. Control over the nature and density of such defects is therefore necessary, are we to fully understand the intrinsic materials properties and exploit them in future device technologies. Here, we show that incorporation of a strontium copper oxide nano-layer strongly reduces the impurity scattering at conducting interfaces in oxide $\text{LaAlO}_3\text{-SrTiO}_3(001)$ heterostructures, opening the door to high carrier mobility materials. We propose that this remote cuprate layer facilitates enhanced suppression of oxygen defects by reducing the kinetic barrier for oxygen exchange in the hetero-interfacial film system. This design concept of

controlled defect engineering can be of significant importance in applications in which enhanced oxygen surface exchange plays a crucial role.

1. Introduction

Advances in material growth have enabled progressive control of the crystalline quality and impurity density of scientifically and technologically important materials. Traditionally, single crystals have been used to study the intrinsic transport properties of complex oxide materials, in which electron-electron correlation effects, electron-lattice interactions and orbital physics are important. Single crystal growth occurs near thermal equilibrium, allowing for a minimal amount of impurities and defects, which is advantageous for transport and other experiments. For example, doped bulk SrTiO_3 crystals exhibit Shubnikov-deHaas (SdH) oscillations^[1] for sufficiently low dopant concentrations (Nb, La, oxygen vacancies). In recent years such quantum oscillations have also been observed in oxide thin films, for example SrRuO_3 ^[2] and SrTiO_3 ^[3], where in particular molecular beam epitaxy has been successful in reducing the presence of extrinsic scatterers in the system. The next step of dimensional reduction to ultra-thin films, with thicknesses down to the atomic scale, has generally led to the degradation of the transport properties^[4]. A perfect model system for the endeavour of combining ultra-thin film thicknesses with high carrier mobilities has been found in the LaAlO_3 - SrTiO_3 oxide heterostructure system^[5,6].

The remarkable electronic transport properties that occur at the interface between the band insulators SrTiO_3 and LaAlO_3 ^[5,6,7] have been attributed to the avoidance of a so-called polar catastrophe, which would result from the polarity discontinuity across the nonpolar/polar interface between SrTiO_3 and LaAlO_3 . In the idealized case, a build-up of electric potential within the LaAlO_3 would trigger the transfer of electrons from the LaAlO_3 surface, through the LaAlO_3 layer, into the SrTiO_3 conduction band for a LaAlO_3 film thickness above a threshold

value of 3-4 unit cells^[8]. Addition of an extra SrTiO₃ capping layer changes the situation dramatically, preventing structural and chemical reconstructions at the LaAlO₃ surface and results in metallic behaviour below this threshold, even down to a single LaAlO₃ unit cell layer^[9,10]. However, to date, although the avoidance of the polar catastrophe is thought by many to lie at the heart of the remarkable physics displayed by these systems, the exact balance between doping via the electronic reconstruction versus from vacancy defects^[11,12,13,14, 15] or cation intermixing^[16,17] is still a matter of ongoing debate.

The exact balance between the different possible sources of electrons residing at or near to the SrTiO₃/LaAlO₃ interface (Figure 1a), results in reported carrier mobilities of only several thousands cm²V⁻¹s⁻¹ [18,19]. For the development of systems based on interfaces with such quality suitable for devices, enhanced mobilities are required. In this context, one important challenge is to reduce the number of activated carriers and to further enhance the mobility, via reduction of (extrinsic) sources of carrier scattering. Oxygen vacancies - when present near the two-dimensional electron gas (2DEG) where the mobile states are hosted - act as point defects and strong charge carrier scatterers, in addition to cation defects as well as interface scattering. Therefore, a proven design strategy to minimize and sideline these almost ubiquitous defects would represent a significant leap forward.

In (ultra)thin-film heterointerface systems, the incorporation of oxygen during cool down of the film stack after growth is crucial to minimize the possible presence of oxygen vacancies. To ensure maximal surface oxygen exchange, three main processes have to be optimal: the reaction of oxygen at the surface of the as-grown film; the transfer from the surface into the crystal; and lastly the transport within the crystal^[20]. In the first step, molecular oxygen is transformed into oxide ions in the outermost layer of the film stack in a reaction involving both electron transfer and ion transfer. The subsequent chemical diffusion of oxide ions into the bulk

involves both ionic and electronic species (i.e. oxygen vacancies and holes), so as to maintain global charge neutrality^[21].

Previous studies of oxygen exchange kinetics in SrTiO₃ (and variations thereof) have shown that this process can be strongly accelerated by addition of a porous Ag or Pt film on top of the SrTiO₃^[22]. This is evidently not a particularly viable process step in the case of heteroepitaxial oxide film stacks such as those studied here. An alternative is to add an overlayer of a layered cuprate such as YBa₂Cu₃O_{7- δ} , at whose surface the reaction steps all occur very fast^[23], meaning that the cuprate essentially delivers pre-formed oxide ions to the layer below^[20] possibly as a consequence of the high energy of the O_{2p}-dominated states at the top of the valence band of the cuprate^[24]. Given the similarity in lattice constants of cuprate systems and the SrTiO₃/LaAlO₃ basis of the heterointerface system, it should be feasible to grow cuprate layers epitaxially on the LaAlO₃, followed by a passivating capping layer of SrTiO₃.

In this study we report on the conversion of these ideas into a successful strategy to minimize the deleterious effects of scattering related to oxygen defects in the LaAlO₃-SrTiO₃ heterointerface. By introducing a remote layer containing strontium copper oxide, as schematically depicted in Figure 1b, the thermally activated carriers found in both the free and SrTiO₃-capped heterointerface systems are suppressed, due to effective, cuprate-mediated avoidance of defects at the LaAlO₃-SrTiO₃ interface. The results are significantly suppressed scattering and greatly enhanced carrier mobilities of the 2DEG states.

2. Results and discussion

To compare the transport properties of SrTiO₃-SrCuO₂-LaAlO₃-SrTiO₃(001) heterostructures with the generally used (SrTiO₃)-LaAlO₃-SrTiO₃(001) interface structures (with or without SrTiO₃ capping layers), SrTiO₃-SrCuO₂-LaAlO₃-SrTiO₃(001) heterostructures

were fabricated by pulsed laser deposition with reflection high-energy electron diffraction (RHEED) control of the growth process (see the methods section for the deposition settings). Figure 2a shows the RHEED analysis during growth of the SrTiO₃-SrCuO₂-LaAlO₃-SrTiO₃(001) heterostructures using pulsed laser deposition. The top panels display the RHEED intensity oscillations during growth of each individual layer indicating successful control on the unit cell (u.c.) scale due to the layer-by-layer growth mode. Results are given for the subsequent growth of a 10 u.c. LaAlO₃ layer, a 1,2 or 3 u.c. SrCuO₂ layer and a 2 u.c. SrTiO₃ toplayer. In Figure 2b the corresponding RHEED patterns are shown for the TiO₂-terminated SrTiO₃ (100) substrate, LaAlO₃ layer, SrCuO₂ layer and SrTiO₃ toplayer (from left to right), showing conservation of surface structure and low surface roughness. After growth, the heterostructures were slowly cooled to room temperature in 6×10^{-2} mbar of oxygen at a rate of 10 °C/minute. X-ray photoelectron spectroscopy indicates that Cu in the SrCuO₂ layer for all heterostructures is in a valence state of 2+ (although small contributions of 3d⁹L configurations cannot be ruled out). In case of SrTiO₃-SrCuO₂-LaAlO₃-SrTiO₃(001) heterostructures grown on SrO-terminated SrTiO₃(100) substrates, the samples were insulating in standard transport measurements. The low level of surface roughness was confirmed by atomic force microscopy (AFM) analysis of the surface of a 2/1/10 SrTiO₃-SrCuO₂-LaAlO₃-SrTiO₃(001) heterostructure. Figure 2c shows the topographic image and the roughness analysis, indicating smooth terraces separated by clear, single unit cell height steps similar to the surface of the initial TiO₂-terminated SrTiO₃ (100) substrate.

Thus, Figure 2 shows we are able to grow SrTiO₃/LaAlO₃ interface systems incorporating a cuprate oxide ion 'supplier' layer, which, as we will go on to show later, removes oxygen vacancies from the region of the 2DEG. In Figure 3, we turn to the transport characterization of these systems. All conducting heterostructures exhibit metallic transport behavior down to 2K. In panel (a) the temperature dependence of the carrier density is shown, which has been

extracted from the Hall coefficient. The uppermost trace (\square) shows the behavior for a 10 unit cell LaAlO_3 layer, which displays a large number of activated carriers ($\sim 1.8 \times 10^{14} \text{ cm}^{-2}$ at room temperature), which freeze out at lower temperatures, resulting in 3×10^{13} carriers per cm^2 at 2K. This carrier freeze out has been observed in previous LaAlO_3 - $\text{SrTiO}_3(001)$ interface studies at an energy scale of 6.0 meV^[9], which is comparable to observations in SrTiO_3 at low La doping^[25]. A typical donor-like defect band located a few meV below the conduction band of SrTiO_3 has been associated with the loss of mobile carriers at low temperatures^[26], schematically indicated in red in the top inset of Figure 3a.

Addition of a 2 unit cell SrTiO_3 cap on a 10 unit cell LaAlO_3 film (\bullet), reduces the room temperature carrier density to just above $1 \times 10^{14} \text{ cm}^{-2}$, and further carrier freeze-out on lowering the temperature brings this system to the same low temperature carrier density as the uncapped system. The solid triangles (stars) show carrier data for one (three) unit cells of SrCuO_2 on a 10 unit cell LaAlO_3 film, with a 2 unit cell SrTiO_3 cap. It is evident that the heterointerfaces containing the remote cuprate layer behave quite differently: the activated carriers are no longer present and both samples with a single and three unit cell thick SrCuO_2 layer the interface systems a fully temperature independent carrier concentration of $\sim 1 \times 10^{13} \text{ cm}^{-2}$ is observed. This means that the cuprate layer has successfully eliminated the defect-related, donor impurity band and the related thermally activated carriers.

The direct consequence of this successful defect engineering is an improvement in carrier mobility, as shown in Figure 3b. The solid symbols show that (2 unit cell) SrTiO_3 -capped film systems comprising 9 or 10 LaAlO_3 unit cells and 1, 2 or 3 SrCuO_2 unit cells all show identical behaviour, with a mobility significantly above that of the cuprate-free films for all temperatures below 150K. At low temperatures, the SrCuO_2 -containing systems reach carrier mobilities up to $5500 \text{ cm}^2\text{V}^{-1}\text{s}^{-1}$, a factor five greater than the control films without the cuprate layer. A

minimum interfacial carrier density of $\sim 7 \times 10^{12} \text{ cm}^{-2}$ was measured for our heterostructures, which can be re-calculated as a minimum volumetric carrier density of $\sim 7 \times 10^{18} \text{ cm}^{-3}$ by taking an upper limit of 10 nm for the thickness of the conducting interfacial region^[27]. Therefore, the observed variations in carrier densities are all in a range well above $\sim 3 \times 10^{17} \text{ cm}^{-3}$, where a maximum carrier mobility for reduced bulk STO is reported^[12] and, thus our observation of an increase in carrier mobility on decreasing the carrier density is in good agreement with previously reported studies. This underpins the hypothesis that the donor states in the cuprate-less systems are a source of significant scattering for the 2DEG states, and that these are effectively eliminated by the introduction of the cuprate inter layer. Indeed, similar samples have been investigated using high-field magnetotransport measurements^[28], and clear 2DEG sub-band structure has been resolved in these data, attesting to the high quality and low scattering the cuprate layer brings about.

The final panel of Figure 3 compares the critical thicknesses of the LaAlO₃ layer required to support metallic conductivity at low temperatures. In the 'first generation', uncapped films of LaAlO₃ on SrTiO₃, the critical thickness is the well-known figure of four unit cells^[8]. On capping the LaAlO₃ with SrTiO₃ ('second generation' systems), the critical thickness sinks to a single unit cell^[9,10]. For the 'third generation' of films of LaAlO₃ on SrTiO₃ with a cuprate interlayer, Figure 3c shows the critical thickness to be 6 unit cells, indicating a great sensitivity of the conducting channel at and near the SrTiO₃/LaAlO₃ interface to the electrostatic and chemical termination of the film stack located on top of the LaAlO₃ layer. The electrical current in transport measurements does not additionally travel a parallel path through the SrCuO₂ layer, as demonstrated by the insulating behaviour in the case of SrTiO₃-SrCuO₂-LaAlO₃-SrTiO₃(001) heterostructures grown on SrO-terminated SrTiO₃(100) substrates (not shown).

Thus far we have explained the design strategy behind the cuprate layer, and the transport data have shown this approach to be successful in boosting the mobility of the carriers in the 2DEG. We now return to the film itself and present data from both transmission electron microscopy and x-ray absorption spectroscopy that hold a surprise in store as regards the structure of the SrCuO₂ inter layer, which proved so effective in reducing the scattering of the 2DEG carriers in the SrTiO₃/LaAlO₃ heterointerface. We have used atomic resolution scanning transmission electron microscopy combined with electron energy loss spectroscopy (STEM-EELS) to investigate the local composition/structure and crystal lattice parameters of the SrTiO₃-SrCuO₂-LaAlO₃-SrTiO₃(001) heterostructures. A high-angle annular dark-field scanning transmission electron microscopy (HAADF-STEM) image of the heterostructure is shown in Figure 4a together with the schematic representation of the individual layers. Clear epitaxial ordering can be observed throughout the complete heterostructure, which is free of structural defects. The observed thicknesses of the individual layers (10 u.c. LaAlO₃ + 1 u.c. SrCuO₂ + 2 u.c. SrTiO₃) measured using STEM match perfectly with the unit-cell controlled growth during PLD deposition monitored using RHEED. A quantitative elemental map of the conducting LaAlO₃-SrTiO₃(001) interface is shown in Figure 4b, and displays data from the La M_{4,5}, Ti L_{2,3} and O K edges, which are enhanced by application of a principal components analysis (PCA) to improve the signal to noise ratio in the EELS spectra. The elemental map and the corresponding La, Ti and O line profiles across the SrTiO₃-LaAlO₃ interface show minimal La diffusion into the SrTiO₃ substrate.^[29]

The HAADF-STEM images are of sufficient quality to enable the analysis of possible local structural variations, via direct determination of lattice parameter changes for each unit cell of the heterointerface film stack. To do this we use atomic position quantification from the aberration corrected HAADF-STEM images, building upon the approach recently introduced by Van Aert et al.^[30,31] for TEM images. This allows position measurements of all atomic

columns with a precision of a few picometers without being restricted by the resolution of the microscope. Figure 5a shows a strip out of a HAADF-STEM image of the SrTiO₃-SrCuO₂-LaAlO₃-SrTiO₃(001) heterostructure. The corresponding graph plots the values of the (pseudo)cubic lattice parameter c (normal to the interface), calculated from the atomic column positions in the HAADF-STEM image together with their 95% confidence intervals. Using the lattice parameter of the single crystal SrTiO₃ (001) substrate (3.905 Å)^[32] as a reference, we determine the c -axis lattice parameter of the grown LaAlO₃ layer (~3.75 Å) to be in good agreement with previous results from X-ray diffraction of such thin films^[7]. Now turning to the cuprate and SrTiO₃ capping layers, the data show that for the former the c -axis lattice parameter is essentially the same as that of the LaAlO₃ at 3.75 Å. The top SrTiO₃ capping layer exhibits a c -axis lattice parameter of ~4 Å. Given stoichiometric transfer of the SrCuO₂ target to the cuprate film, two possible Cu-O networks are possible in the sandwich between the LaAlO₃ and SrTiO₃ cap. Firstly, the 'infinite layer' structure, comprising of a single CuO₂ plane (see lower part of Figure 5c) and out-of-plane Sr ions, which in bulk form has a c -axis lattice parameter of 3.4 Å^[33]. The second possibility would be an arrangement in which the CuO₄-plaquettes lie in the plane of the film normal, and are arranged as a corner sharing chain, as sketched in the upper part of Figure 5c. This would mean - compared to the infinite layer structure - that oxygen atoms are moving to out-of-plane positions, giving rise to an effective Cu-O and Sr-O layering along the c -direction. As a bulk crystal, this Cu-O network can be found in Sr₂CuO₃, and translated to the axis system of the film stack, this kind of corner sharing chain system would possess a c -axis lattice parameter of ~3.9 Å^[34]. Based on these observation there is strong support for the plaquette arrangement over the infinite layer. Furthermore, in the field of view of the STEM images, there is no detectable change in the average of the lattice parameter parallel to the interface, consistent with a high-quality, pseudomorphically constrained thin film.

Seeing as the ultrathin SrCuO₂ layer is too sensitive to the electron beam to be investigated using EELS in the TEM, we have used polarization-dependent X-ray absorption at the Cu-L₃ edge to investigate both 2/1/4 and 2/1/6 SrTiO₃-SrCuO₂-LaAlO₃-SrTiO₃(001) heterostructures, with the data for a 2/1/4 sample being shown in Figure 5b. The Cu-L₃ edge probes Cu2p→Cu3d excitations and, for a divalent system composed of CuO₄-plaquettes the only available final state (2p⁵3d¹⁰) involves the Cu3d_{x²-y²} orbital, which lies in the plane of the plaquette (see Figure 5c). Therefore, in the context of the issue at hand, the dichroism in the X-ray absorption between an experiment placing the **E**-vector in and perpendicular to the film plane will provide information on the structure of the cuprate layer. For the infinite layer structure, **E**||film would yield a strong so-called white line (2p⁶3d⁹→2p⁵3d¹⁰), and for the **E**-vector pointing out of the film plane, almost no intensity would be expected^[35]. For the Cu-O chain comprised of edge-sharing plaquettes, bulk Sr₂CuO₃ is a good reference material, and again here the Cu-L₃ white line is strong for **E** in the plane of the plaquettes and ten times weaker for **E** perpendicular to the plaquettes^[36]. For the data shown in Figure 5b, the X-rays are incident at a grazing angle to the film-stack, with either **E**||film (linear vertical polarization as shown in Figure 5c) or **E** perpendicular to the film (linear horizontal polarization in Figure 5c). As Figure 5b makes very clear, the Cu-L₃ white line is only a little stronger for **E**||film than for **E**⊥film. This rules out a pure infinite layer structure for the SrCuO₂, in agreement with the STEM data of Figure 5a. Over the macroscopic area of 0.1 x 2.6 mm² probed by the grazing incidence XAS experiment - if we assume equal proportions of Cu-O chains running along the two in-plane axes of the film - the data of Figure 5b would be consistent with more than 60% of the CuO₄-plaquettes in a 'standing', or chain-like configuration, and only 40% arranged as in the infinite layer structure.

Recent DFT-based calculations^[37] have studied the question of the lowest energy structure for such ultrathin cuprate layers in film stacks such as those under investigation here, coming to

the conclusion that the SrCuO₂ should be present in the form of edge-sharing chain structures, with the thin film normal lying in the plane of the CuO₄-plaquettes. This expectation matches well with both the c-axis distances observed in the STEM data (Figure 5a) as well as with the fact that only weak linear dichroism is observed in the polarized X-ray absorption data (Figure 5b). A preliminary conclusion would be to correlate the chain-like structure of the cuprate layer to the enhanced oxygen uptake, which needs more detailed analysis.

To determine the mechanism of the remote strontiumcopperoxide layer to eliminate defects, additional experiments have been performed. An intermediate cool down step to room temperature in between the depositions of LaAlO₃ and SrCuO₂ was applied. Due to this additional step, thermally activated carriers were observed, similar to those interface structures without a SrCuO₂ layer. This observation also excludes intermixing as the possible cause for creation of defects. In order to further investigate the phenomenology of the strontium copper oxide layer in the elimination of defects, we have performed two additional sets of experiments. Firstly, a series of heterostructures have been fabricated under different oxygen partial pressures during the growth of the LaAlO₃ layer. Figure 6a displays carrier concentration data showing that over a wide oxygen pressure regime, from 10⁻³ to 10⁻⁶ mbar, the incorporation of a SrCuO₂ layer results in the removal of the thermally activated carriers and their associated donor defect levels, leaving a constant low carrier density over the entire temperature range (excluding the effects of oxygen defects in the bulk of the substrate, as reported previously for lowest oxygen partial pressures^[5,12]). Interestingly, carrier mobilities in excess of 50.000 cm²V⁻¹s⁻¹ are observed for the 3rd generation 2DEGs grown in the lowest oxygen partial pressures (Figure 6b).

These results demonstrate a marked dependence of the observed carrier mobility on the oxygen pressure during growth of the heterostructures with a SrCuO₂ layer. The differences between those samples with and without the cuprate interlayer allow us to make a separation of

the effects on the final carrier mobility observed for the complete heterostructure system: the initial oxidation level of the heterostructure/substrate, the disorder induced by bulk diffusion within the single-crystalline substrate and possibly by the growth mode of the deposited material on the substrate surface. In the following, each of these factors is described in detail.

The oxygen pressure during deposition will determine the initial oxidation level of the LaAlO₃ thin film and interface during growth. It is known that in oxide materials oxygen vacancies can easily be formed when a low oxygen pressure is chosen in combination with high temperatures. Therefore, immediately after the growth of the LaAlO₃, some amount of oxygen vacancies can be present, and that this amount can be considerable, depending on the actual oxygen pressure used during growth. These vacancies could in part be eliminated during cool-down to room temperature. However, transport measurements for samples without the cuprate interlayer generally show the presence of activated carriers (e.g. see Fig. 6), indicating that oxygen vacancies still exist for all interfaces grown in oxygen pressures in the range of 10⁻⁶ – 10⁻³ mbar. These samples have not been fully oxidized due to a limitation in the oxygen surface exchange. The remaining oxygen vacancies - which are charged impurities - act as scattering centers, limiting the mobility of the mobile charge carriers.

The bulk diffusion within the substrate crystal is also determined by the oxygen pressure used. It is known that Sr-diffusion within a SrTiO₃ substrate crystal is minimized at low oxygen pressures^[38]. Therefore, for oxide growth at low oxygen pressures such as 10⁻⁶ mbar a highly ordered TiO₂-terminated surface of the SrTiO₃ crystal can be maintained, resulting in a highly ordered LaAlO₃-SrTiO₃ interface. In contrast, for higher oxygen pressures of 10⁻³ mbar some Sr-diffusion to the SrTiO₃ surface could lead to a mixed-termination of TiO₂ and SrO, resulting in more disorder at the LaAlO₃-SrTiO₃ interface. The disorder will influence the scattering of the mobile charge carriers, and therefore, lower the carrier mobility for high oxygen pressures of 10⁻³ mbar. Additionally, the growth mode of LaAlO₃ on a SrTiO₃ substrate exhibits a

transition from two-dimensional, layer-by-layer growth at low oxygen pressures to island growth at high oxygen pressures^[7]. The actual growth mode will influence the amount of disorder, and therefore the crystallinity, of the final LaAlO₃ thin film and thus the interfacial region. Local defects in the crystal structure will have a strong influence on the scattering of mobile charge carriers being transported in the 2D-layer at and near to the interface.

In the work presented here, we use a cuprate interlayer to dramatically enhance the oxygen surface exchange, thereby improving the oxidation of the whole system during cool-down and consequently reducing the amount of oxygen vacancies in our samples. That this factor is operative is clear in the elimination of activated carriers (see Fig. 3), which leads to a significant decrease in the number of transport-active charge carriers observed at low temperature from values between $2.0\text{-}2.7 \times 10^{13} \text{ cm}^{-2}$ to $0.7\text{-}1.4 \times 10^{13} \text{ cm}^{-2}$ when this cuprate layer is introduced. This effect is clearly present for all cuprate-containing samples grown in oxygen pressures in the range of $10^{-6} - 10^{-3}$ mbar (see Fig. 6a).

At the same time, the addition of the cuprate layer leads to an increase in the carrier mobility, confirming the reduction of scattering by oxygen vacancies. The actual carrier mobility of the whole system depends on the remaining scattering of the mobile charge carriers from disorder at the interface caused by the growth mode and bulk diffusion at different oxygen pressures. The removal of the masking effect on the mobility due to oxygen-vacancy induced scattering achieved by adding the cuprate layer now enables us to zoom in on the next sources of scattering, which are clearly dependent on the oxygen pressure during growth of the LaAlO₃-SrTiO₃ interface. Growth in the highest oxygen pressure of 10^{-3} mbar results in a degree of disorder at the interface and a maximum carrier mobility of about $5500 \text{ cm}^2\text{V}^{-1}\text{s}^{-1}$. The intermediate oxygen pressure of 10^{-5} mbar gives rise to less disorder and a carrier mobility up to about $9000 \text{ cm}^2\text{V}^{-1}\text{s}^{-1}$. The lowest oxygen pressure of 10^{-6} mbar gives a region at/near the interface with the lowest disorder, which in turn leads to a very high low-temperature carrier

mobility of about $50.000 \text{ cm}^2\text{V}^{-1}\text{s}^{-1}$. Thus, this research takes an important step in showing that the cuprate layer is crucial in the enhancement of the surface oxygen exchange so as to eliminate oxygen vacancies. The final carrier mobilities are then limited by remnant disorder, which can be minimized by growing at low oxygen pressure, such that low bulk diffusion and an ideal layer-by-layer growth give a highly ordered interface with low scattering, and therefore, a high carrier mobility.

A second set of additional experiments involved studying the influence of introducing various different cuprate layers besides SrCuO_2 such as CuO , $\text{YBa}_2\text{Cu}_3\text{O}_{7-\delta}$ and $\text{La}_{1.85}\text{Sr}_{0.15}\text{CuO}_4$ (data not shown). All of these cuprate layers showed the same strong reduction of impurity scattering signaled by the absence of the carrier freeze-out at low temperatures. Introduction of LaTiO_3 or LaNiO_3 layers instead of the cuprate layer did not have the same effect, demonstrating the particular efficacy of cuprate layers in enhancing the oxygen incorporation, thereby strongly reducing carrier scattering from oxygen vacancies at the interface.

Finally, it is also important to note that the SrTiO_3 - SrCuO_2 - LaAlO_3 - $\text{SrTiO}_3(001)$ heterostructures showed metallic behaviour down to 60 mK without any signature of the superconductivity which has been observed previously in delta-doped SrTiO_3 [39] and at the LaAlO_3 - SrTiO_3 interface [27]. Seeing as the 2DEG we see in action here (the quantum oscillations of which are studied in detail in Ref. 28) is outside of the superconducting regime in the samples discussed here, this makes it clear that a high mobility quasi-2D electron gas and superconductivity can be observed independently in SrTiO_3 , unlike has been concluded in an earlier report [39].

3. Conclusion

In conclusion, the introduction of a remote SrCuO₂ layer in the SrTiO₃-capped LaAlO₃-SrTiO₃ interface system strongly enhanced the electron mobility by eliminating the negative influence of defect states. This suppression of oxygen defects in oxide hetero-interfacial film systems enables the fundamental study of previously inaccessible quantum phenomena in complex oxide 2DEGs. Furthermore, this design concept of controlled defect engineering can be of significant importance in applications in which enhanced oxygen surface exchange plays a crucial role.

4. Experimental

Atomically smooth TiO₂-terminated SrTiO₃(100) substrates were prepared by a combined HF- etching/anneal treatment. All substrates had vicinal angles of ~0.1°. Single-crystal LaAlO₃ and SrTiO₃ targets as well as a stoichiometric SrCuO₂ target were ablated at a laser fluence of 1.3 J/cm² and a repetition rate of 1 Hz. During growth, the substrate was held at 850 °C in an oxygen environment at 2x10⁻³ mbar for LaAlO₃ (except when mentioned otherwise, while for SrCuO₂ and SrTiO₃ the conditions were adjusted to 650 °C and 6x10⁻² mbar. The sheet carrier density and mobility were determined by a Hall measurement using a Van der Pauw configuration.

Atomic resolution STEM-EELS and HAADF-STEM measurements were performed using the Qu-Ant-EM microscope at the University of Antwerp consisting of a probe-corrected TITAN G2 80-300 (FEI) instrument equipped with a GIF Quantum spectrometer for electron energy loss spectroscopy (EELS). The effective probe-size during acquisition is approximately equal to 1.5 Å. Low loss and core-loss spectra are recorded quasi-simultaneously by using the spectrometer in dual EELS mode. The collection and convergence angle are $\alpha = 21$ mrad and $\beta = 25$ mrad, respectively. The energy resolution in STEM-EELS was approximately equal to 1.2 eV.

X-ray absorption measurements were carried out at the Cu-L_{2,3} edges using linearly polarised synchrotron radiation from the UE56/2-PGM-2 undulator beamline at the BESSY-II electron storage ring at the Helmholtz-Zentrum Berlin. The absorption cross-section was monitored using the drain current, and normalized in the pre-edge region. The films studied were transferred from the UHV PLD chamber in Twente to the XAS chamber at the light source in Berlin using a UHV sample transfer chamber, in which the pressure was maintained under 5×10^{-10} mbar at all times. Linearly polarized synchrotron radiation (spot-size 900 μm horizontal, 100 μm vertical) impinged on the film at an incidence angle of 20 degrees, with an energy bandwidth of 350 meV. At grazing incidence, selecting p-polarized light puts the E-vector of the x-rays in the plane of the film stack, whereas selecting s-polarized light placed the E-vector close to the normal of the heterointerface film structure.

Acknowledgements

This work is supported by the Netherlands Organization for Scientific Research (NWO) through VENI (M.H.), VIDI (A.B., G.R.) and VICI (H.H.) grants and by the Dutch Foundation for Fundamental Research on Matter (FOM) through the InterPhase program. We are grateful for experimental support during the XAS experiments to Christian Schuessler-Langeheine and Christoph Trabant, whose experimental station is funded by the BMBF (05K10PK2). Access to HZB was also supported by the EU (7th FP, no. 226716). The Qu-Ant-EM microscope was partly funded by the Hercules fund from the Flemish Government. G.V.T. acknowledges funding from the European Research Council, ERC grant N°246791 – COUNTATOMS and J.V. acknowledges funding from the ERC Starting Grant 278510 VORTEX. All authors acknowledge funding by the European Union Council under the 7th Framework Program (FP7) grant nr NMP3-LA-2010-246102 IFOX and the Research Foundation Flanders (FWO, Belgium).

Received: ((will be filled in by the editorial staff))

Revised: ((will be filled in by the editorial staff))

Published online: ((will be filled in by the editorial staff))

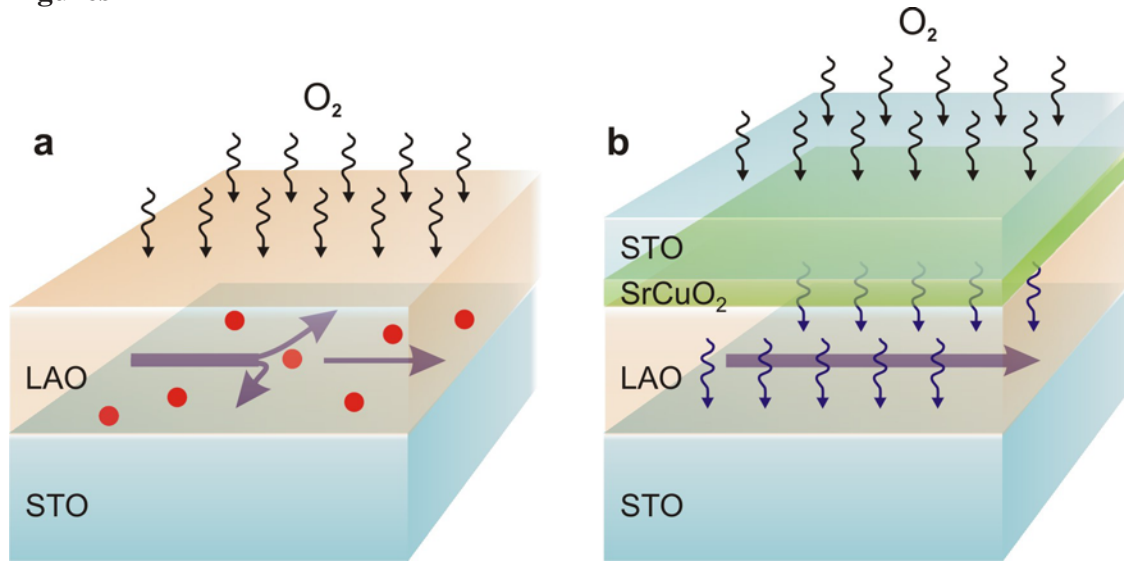
Figures

Figure 1 | Schematic representation of enhanced oxygen incorporation in SrTiO₃-(SrCuO₂)-LaAlO₃-SrTiO₃(001) heterostructures. (a) The limited oxygen surface exchange causes the presence of oxygen vacancies at an LaAlO₃-SrTiO₃(001) interface leading to defect scattering. **(b)** The introduction of a SrCuO₂ layer enhances the oxygen exchange and eliminates the oxygen vacancies resulting in reduced scattering of the carriers at the interface. Carrier transport at the interface is indicated by blue arrows, while the oxygen vacancies are represented by red points.

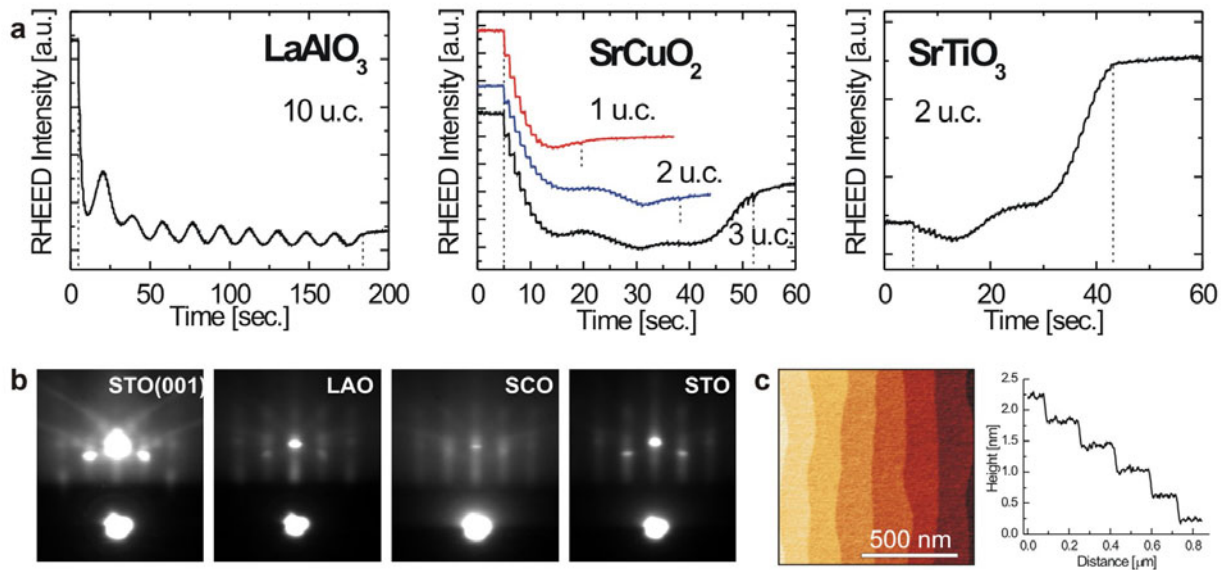


Figure 2 | Thin film growth of SrTiO_3 - SrCuO_2 - LaAlO_3 - $\text{SrTiO}_3(001)$ heterostructures by pulsed laser deposition. (a) RHEED intensity monitoring during growth of subsequently a 10 u.c. LaAlO_3 layer, a 1,2 or 3 u.c. SrCuO_2 layer and a 2 u.c. SrTiO_3 toplayer. Clear intensity oscillations indicate layer-by-layer growth of single unit cells. Dashed lines indicate start/stop of laser pulses. **(b)** RHEED patterns after growth of each consecutive layer. **(c)** Surface topography and roughness analysis of a 2/1/10 SrTiO_3 - SrCuO_2 - LaAlO_3 - $\text{SrTiO}_3(001)$ heterostructure by AFM of a $1 \times 1 \mu\text{m}^2$ area.

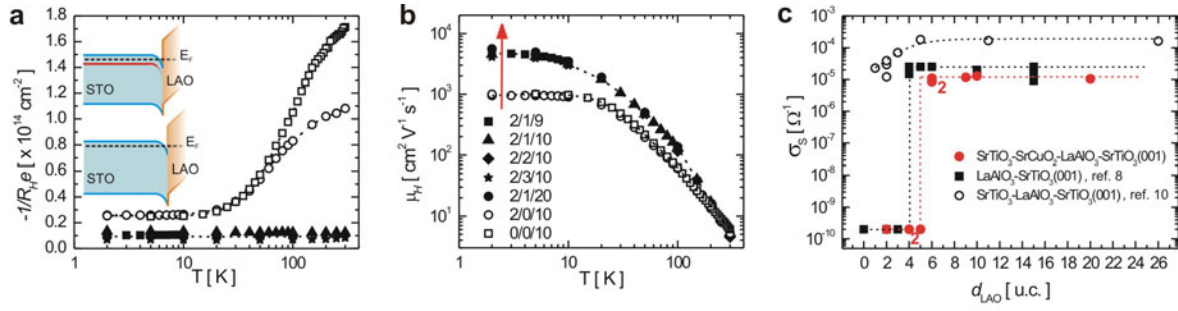


Figure 3 | Transport properties of SrTiO₃-(SrCuO₂)-LaAlO₃-SrTiO₃(001) heterostructures. (a) With or without a SrCuO₂ layer. Temperature dependence of $-1/R_{\text{HE}}$, indicating the carrier density, for heterostructures with (closed symbols) and without (open symbols) a SrCuO₂ layer. The corresponding bandstructures are schematically represented in the insets. When the additional SrCuO₂ layer is introduced, the commonly observed defect donor band (shown in red in the top inset) is eliminated (bottom inset). (b) Corresponding temperature dependence of Hall mobility μ_{H} . Various heterostructure configurations are given, for example 2/1/10 SrTiO₃-SrCuO₂-LaAlO₃-SrTiO₃(001) represents a 2 u.c. SrTiO₃ toplayer with a 1 u.c. SrCuO₂ layer and a 10 u.c. LaAlO₃ layer on a SrTiO₃ substrate; in the heterostructure indicated with 2/0/10 SrTiO₃-SrCuO₂-LaAlO₃-SrTiO₃(001), the SrCuO₂ layer is absent. (c) Sheet conductance dependence on LaAlO₃ layer thickness at 300 K. Heterostructures with a SrCuO₂ layer exhibit a sharp insulator-metal transition at a LaAlO₃ layer thickness of 6 unit cells. Data for LaAlO₃-SrTiO₃(001) single interfaces from Thiel *et al.*⁸ and for coupled interfaces in SrTiO₃-LaAlO₃-SrTiO₃(001) heterostructures from Pentcheva *et al.*¹⁰ are also shown for comparison.

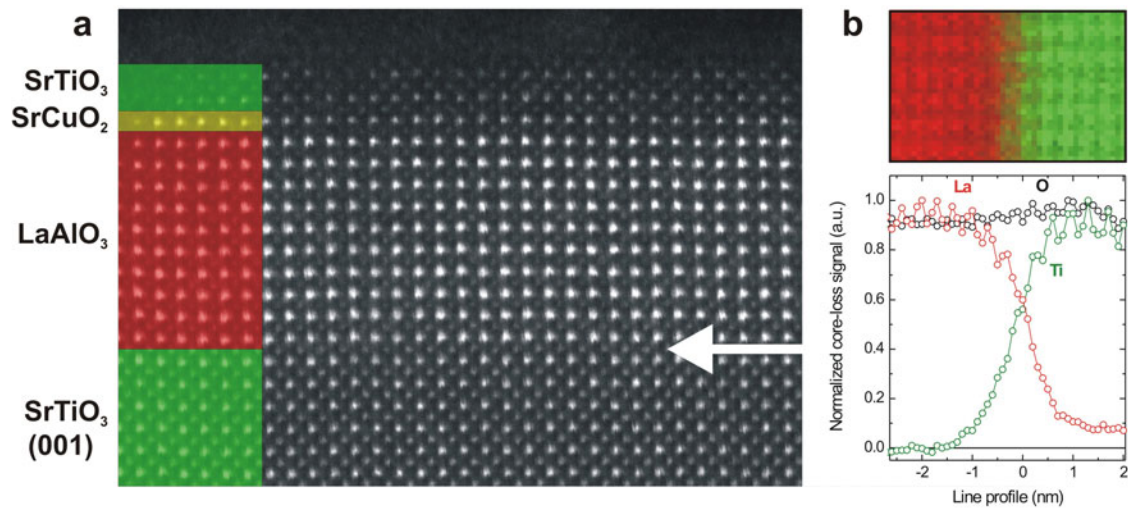


Figure 4 | Quantitative scanning transmission electron microscopy analysis of the atomic stacking sequences in SrTiO₃-SrCuO₂-LaAlO₃-SrTiO₃(001) heterostructures. (a) HAADF-STEM image of the heterostructure along the [001] zone axis, together with the schematic representation of the individual layers. **(b)** EELS analysis of the conducting LaAlO₃-SrTiO₃(001) interface within the heterostructure showing normalized core-loss signals for La M_{4,5} (red), Ti L_{2,3} (green) and O K (black) edges.

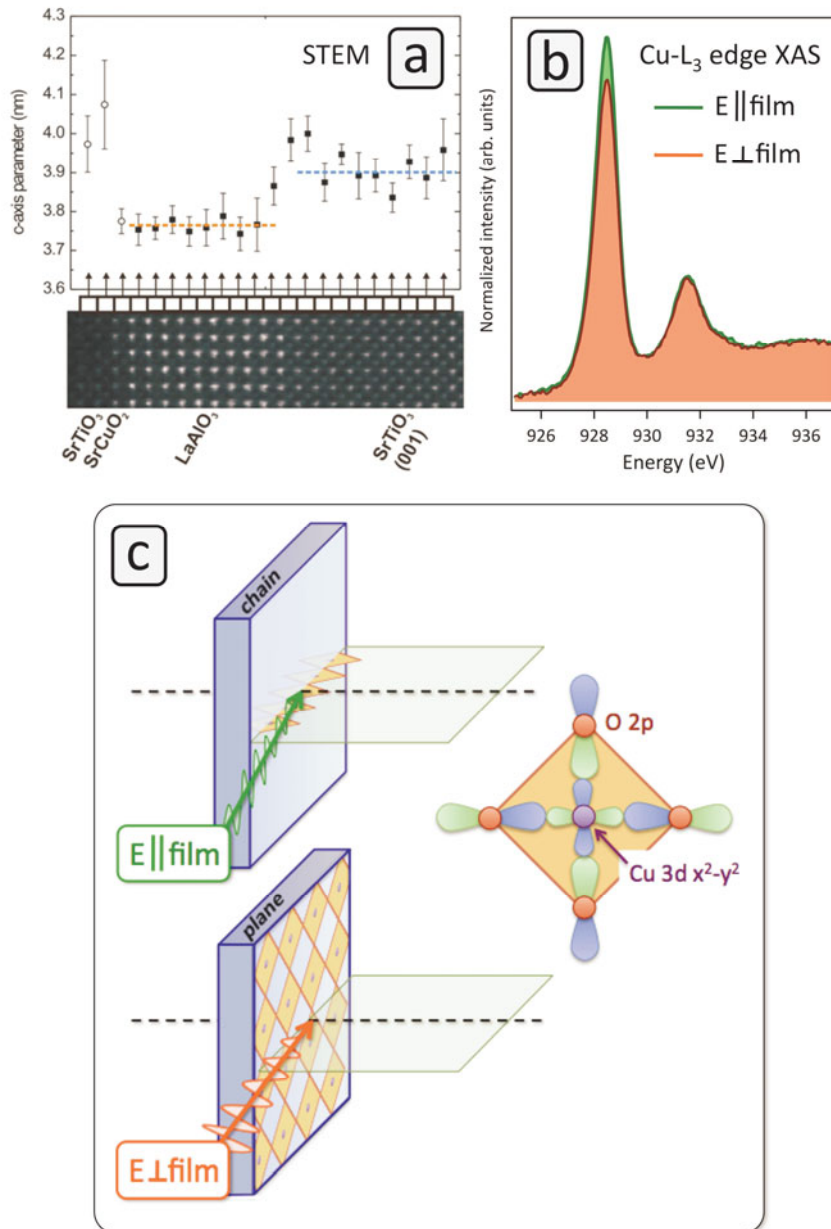


Figure 5 | Structural ordering of the incorporated SrCuO₂ layer. (a) Quantification by STEM of the *c*-axis parameter for the SrTiO₃-SrCuO₂-LaAlO₃-SrTiO₃(001) heterostructure using the single crystalline SrTiO₃ (001) substrate as a calibration standard. The distances between the atomic planes in LaAlO₃ and SrTiO₃(001) are indicated as closed squares, while open circles are used for the SrCuO₂ and SrTiO₃ toplayer. Furthermore, 95% confidence intervals are shown. (b) Linear dichroism in X-ray absorption at the Cu-L₃ absorption edge for a 2/1/4 SrTiO₃-SrCuO₂-LaAlO₃-SrTiO₃(001) heterostructure. The white line at 928.5 eV is only 9% more intense for the polarization vector in the plane of the film, compared to

perpendicular. (c) Simplified sketch of possible SrCuO_2 structures. Upper: chain-like, such that the $E \parallel$ film case places the E-vector out of the CuO_4 -plaquettes. Lower: plane-like, such that only the E perpendicular to the film case places the E-vector out of the CuO_4 -plaquettes. Right: cartoon of the low lying electronic states in a cuprate CuO_4 plaquette, showing the $\text{Cu}3d_{x^2-y^2}$ and $\text{O}2p_{x,y}$ orbitals. These states are the first electron addition states for a divalent cuprate and are polarized in the plaquette.

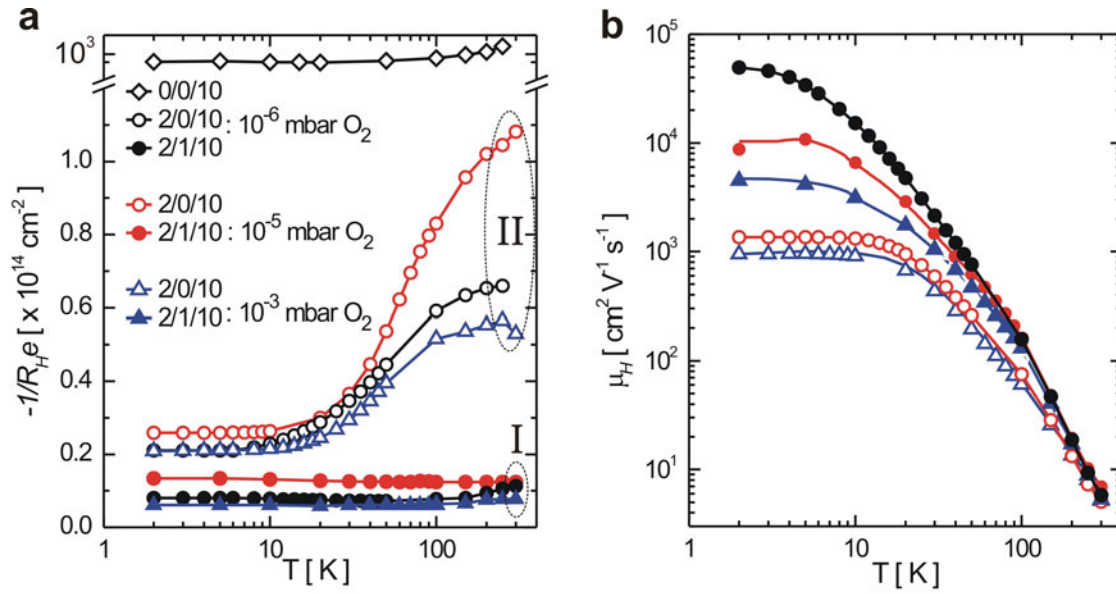


Figure 6 | Mobility enhancement by defect engineering over a wide oxygen pressure regime. Temperature dependence of (a) $-1/R_{He}$, indicating the carrier density, and (b) Hall mobility μ_H for SrTiO₃-(SrCuO₂)-LaAlO₃-SrTiO₃(001) heterostructures with (group I: closed symbols) and without (group II: open symbols) a SrCuO₂ layer for various oxygen growth pressures. The corresponding Hall resistance versus magnetic field exhibits linear dependence for the complete temperature range (2-300 K), indicating the presence of a single type of carrier. The carrier mobilities of the 2/0/10 and 0/0/10 (10⁻⁶ mbar O₂) samples were excluded as nonlinear dependence is observed in the former and bulk conductivity in the latter.

References

-
- ¹ H.P.R. Frederikse, W.R. Hosler, W.R. Thurber, J. Babiskin, and P.G. Siebenmann, Shubnikov—de Haas Effect in SrTiO₃. *Phys. Rev.* **1967**, 158, 775 - 778.
- ² A.P. Mackenzie, J.W. Reiner, A.W. Tyler, L.M. Galvin, S.R. Julian, M.R. Beasley, T.H. Geballe, and A. Kapitulnik, Observation of quantum oscillations in the electrical resistivity of SrRuO₃. *Phys. Rev. B* **1998**, 58, R13318.
- ³ J. Son, P. Moetakef, B. Jalan, O. Bierwagen, N.J. Wright, R. Engel-Herbert, and S. Stemmer, Epitaxial SrTiO₃ films with electron mobilities exceeding 30,000 cm²V⁻¹s⁻¹. *Nat. Mater.* **2010**, 9, 482 - 484.
- ⁴ G. Koster, L. Klein, W. Siemons, G. Rijnders, J. Dodge, C. Eom, D. Blank, and M. Beasley, Structure, physical properties, and applications of SrRuO₃ thin films. *Rev. Mod. Phys.* **2012**, 84, 253–298.
- ⁵ A. Ohtomo, and H.Y. Hwang, A high-mobility electron gas at the LaAlO₃/SrTiO₃ heterointerface. *Nature* **2004**, 427, 423 - 426.
- ⁶ A. Ohtomo, and H.Y. Hwang, Corrigendum: a high-mobility electron gas at the LaAlO₃/SrTiO₃ heterointerface. *Nature* **2006**, 441, 120.
- ⁷ M. Huijben, A. Brinkman, G. Koster, G. Rijnders, H. Hilgenkamp, and D.H.A. Blank, Structure–property relation of SrTiO₃/LaAlO₃ Interfaces. *Adv. Mater.* **2009**, 21, 1665 – 1677.
- ⁸ S. Thiel, G. Hammerl, A. Schmehl, C.W. Schneider, and J. Mannhart, Tunable quasi-two-dimensional electron gases in oxide heterostructures. *Science* **2006**, 313, 1942 – 1945.
- ⁹ M. Huijben, G. Rijnders, D.H.A. Blank, S. Bals, S. van Aert, J. Verbeeck, G. van Tendeloo, A. Brinkman, and H. Hilgenkamp, Electronically coupled complementary interfaces between perovskite band insulators. *Nat. Mater.* **2006**, 5, 556 - 560.
- ¹⁰ R. Pentcheva, M. Huijben, K. Otte, W.E. Pickett, J.E. Kleibeuker, J. Huijben, H. Boschker, D. Kockmann, W. Siemons, G. Koster, H.J.W. Zandvliet, G. Rijnders, D.H.A. Blank, H. Hilgenkamp, and A. Brinkman, Parallel electron-hole bilayer conductivity from electronic interface reconstruction. *Phys. Rev. Lett.* **2010**, 104, 166804.
- ¹¹ A. Brinkman, M. Huijben, M. van Zalk, J. Huijben, U. Zeitler, J.C. Maan, W.G. van der Wiel, G. Rijnders, D.H.A. Blank, and H. Hilgenkamp, Magnetic effects at the interface between non-magnetic oxides. *Nat. Mater.* **2007**, 6, 493 - 496.
- ¹² G. Herranz, M. Basletić, M. Bibes, C. Carrétéro, E. Tafra, E. Jacquet, K. Bouzehouane, C. Deranlot, A. Hamzić, J.-M. Broto, A. Barthélémy, and A. Fert, High mobility in LaAlO₃/SrTiO₃ heterostructures: origin, dimensionality, and perspectives. *Phys. Rev. Lett.* **2007**, 98, 216803.

- ¹³ A. Kalabukhov, R. Gunnarsson, J. Börjesson, E. Olsson, T. Claeson, and D. Winkler, Effect of oxygen vacancies in the SrTiO₃ substrate on the electrical properties of the LaAlO₃/SrTiO₃ interface. *Phys. Rev. B* **2007**, 75, 121404.
- ¹⁴ W. Siemons, G. Koster, H. Yamamoto, W.A. Harrison, G. Lucovsky, T.H. Geballe, D.H.A. Blank, and M.R. Beasley, Origin of charge density at LaAlO₃ on SrTiO₃ heterointerfaces: possibility of intrinsic doping. *Phys. Rev. Lett.* **2007**, 98, 196802.
- ¹⁵ Y. Chen, N. Pryds, J. E. Kleibecker, G. Koster, J. Sun, E. Stamate, B. Shen, G. Rijnders, and S. Linderoth, “Metallic and insulating interfaces of amorphous SrTiO₃-based oxide heterostructures,” *Nano Letters* **2011**, 11, 3774–3778.
- ¹⁶ A.S. Kalabukhov, Yu.A. Boikov, I.T. Serenkov, V.I. Sakharov, V.N. Popok, R. Gunnarsson, J. Börjesson, N. Ljustina, E. Olsson, D. Winkler, and T. Claeson, Cationic disorder and phase segregation in LaAlO₃/SrTiO₃ heterointerfaces evidenced by medium-energy ion spectroscopy. *Phys. Rev. Lett.* **2009**, 103, 146101.
- ¹⁷ S.A. Chambers, M.H. Engelhard, V. Shutthanandan, Z. Zhu, T.C. Droubay, L. Qiao, P.V. Sushko, T. Feng, H.D. Lee, T. Gustafsson, E. Garfunkel, A.B. Shah, J.-M. Zuo, and Q.M. Ramasse, Instability, intermixing and electronic structure at the epitaxial LaAlO₃/SrTiO₃(001) heterojunction. *Surf. Sci. Rep.* **2010**, 65, 317–352.
- ¹⁸ M. Ben Shalom, A. Ron, A. Palevski, and Y. Dagan, Shubnikov-De Haas Oscillations in SrTiO₃/LaAlO₃ Interface. *Phys. Rev. Lett.* **2010**, 105, 206401.
- ¹⁹ A.D. Caviglia, S. Gariglio, C. Cancellieri, B. Sacépé, A. Fête, N. Reyren, M. Gabay, A.F. Morpurgo, and J.-M. Triscone, Two-dimensional quantum oscillations of the conductance at LaAlO₃/SrTiO₃ Interfaces. *Phys. Rev. Lett.* **2010**, 105, 236802.
- ²⁰ R. Merkle, and J. Maier, How is oxygen incorporated into oxides? A comprehensive kinetic study of a simple solid-state reaction with SrTiO₃ as model material, *Angew. Chem. Int. Ed.* **2008**, 47, 3874-3894.
- ²¹ R. Merkle, R. and J. Maier, The significance of defect chemistry for the rate of gas-solid reactions: three examples, *Top. Catal.* **2006**, 38, 141-145.
- ²² M. Leonhardt, R.A. De Souza, J. Claus, J. and J. Maier, Surface kinetics of oxygen incorporation into SrTiO₃, *J. Electrochem. Soc.* **2002**, 149, J19-J26.
- ²³ I. Denk, W. Münch, and J. Maier, Partial conductivities in SrTiO₃: Bulk polarization experiments, oxygen concentration cell measurements, and defect-chemical modeling, *J. Am. Ceram. Soc.* **1995**, 78, 3265-3272.
- ²⁴ S. Yunoki, A. Moreo, and E. Dagotto, Electron doping of cuprates via interfaces with manganites. *Phys. Rev. B* **2007**, 76, 064532.
- ²⁵ T. Okuda, K. Nakanishi, S. Miyasaka, and Y. Tokura, Large thermoelectric response of metallic perovskites: Sr_{1-x}La_xTiO₃ (0<x<0.1). *Phys. Rev. B* **2001**, 63, 113104.

- ²⁶ O.N. Tufte, and P.W. Chapman, Electron mobility in semiconducting strontium titanate. *Phys. Rev.* **1967**, 155, 796 - 802.
- ²⁷ N. Reyren, S. Thiel, A.D. Caviglia, L. Fitting Kourkoutis, G. Hammerl, C. Richter, C.W. Schneider, T. Kopp, A.-S. Rüetschi, D. Jaccard, M. Gabay, D.A. Muller, J.-M. Triscone, and J. Mannhart, Superconducting interfaces between insulating oxides. *Science* **2007**, 317, 1196-1199.
- ²⁸ A. McCollam, S. Wenderich, M.K. Kruize, V.K. Guduru, H.J.A. Molegraaf, M. Huijben, G. Koster, D.H.A. Blank, G. Rijnders, A. Brinkman, H. Hilgenkamp, U. Zeitler, J.C. Maan, Quantum oscillations and subband properties of the two-dimensional electron gas at the LaAlO₃/SrTiO₃ interface, **2012**, arXiv:1207.7003.
- ²⁹ Here we concentrate on the conducting LaAlO₃-SrTiO₃(001) interface as the electron beam causes damage to the SrCuO₂ layer during the prolonged exposure required for such STEM-EELS data.
- ³⁰ S. Van Aert, S. Turner, R. Delville, D. Schryvers, G. Van Tendeloo, and E.K.H. Salje, Direct observation of ferroelectricity at ferroelastic domain boundaries in CaTiO₃ by electron microscopy. *Adv. Mater.* **24**, 523-527 (2012).
- ³¹ S. Bals, S. Van Aert, G. Van Tendeloo, and D. Ávila-Brandé, Statistical estimation of atomic positions from exit wave reconstruction with a precision in the picometer range. *Phys. Rev. Lett.* **2006**, 96, 096106.
- ³² Yu.A. Abramov, V.G. Tsirelson, V.E. Zavodnik, S.A. Ivanov, and I.D. Brown, The chemical bond and atomic displacements in SrTiO₃ from X-ray diffraction analysis, *Acta Cryst. B* **1995**, 51, 942.
- ³³ M. Takano, Y. Takeda, H. Okada, M. Miyamoto, and T. Kusaka, ACuO₂ (A: alkaline earth) crystallizing in a layered structure, *Physica C* **1989**, 159, 375.
- ³⁴ Y. Matsushita, Y. Oyama, M. Hasegawa, and H. Takei, Growth and Structural Refinement of Orthorhombic SrCuO₂ Crystals, *J. Solid State Chem.* **1995**, 114, 289-293.
- ³⁵ M.S. Golden, C. Dürr, A. Koitzsch, S. Legner, Z. Hu, S. Borisenko, M. Knupfer, and J. Fink, The electronic structure of cuprates from high energy spectroscopy, *J. Electron Spectrosc.* **2001**, 117-118, 203-222.
- ³⁶ R. Neudert, S.-L. Drechsler, J. Málek, H. Rosner, M. Kielwein, Z. Hu, M. Knupfer, M. S. Golden, J. Fink, N. Nücker, M. Merz, S. Schuppler, N. Motoyama, H. Eisaki, S. Uchida, M. Domke and G. Kaindl, Four-band extended Hubbard Hamiltonian for the one-dimensional cuprate Sr₂CuO₃: Distribution of oxygen holes and its relation to strong intersite Coulomb interaction, *Phys. Rev. B* **2000**, 62, 10752.
- ³⁷ Z. Zhong, G. Koster, and P.J. Kelly, Prediction of thickness limits of ideal polar ultrathin films, *Phys. Rev. B* **2012**, 85, 121411(R).
- ³⁸ R. Moos and K. H. Hardtl, Defect chemistry of donor-doped and undoped strontium titanate ceramics between 1000°C and 1400°C, *J. Am. Ceram. Soc.* **1997**, 80, 2549.
- ³⁹ Y. Kozuka, M. Kim, C. Bell, B.G. Kim, Y. Hikita, and H.Y. Hwang, Two-dimensional normal-state quantum oscillations in a superconducting heterostructure. *Nature* **2009**, 462, 487 - 490.

Info for table of contents**Defect engineering in oxide heterostructures by enhanced oxygen surface exchange**

M. Huijben, G. Koster, M.K. Kruize, S. Wenderich, J. Verbeeck, S. Bals, E. Slooten, B. Shi, H.J.A. Molegraaf, J.E. Kleibeuker, S. Van Aert, J.B. Goedkoop, A. Brinkman, D.H.A. Blank, M.S. Golden, G. Van Tendeloo, H. Hilgenkamp, and G. Rijnders

Defect engineering of conducting interfaces in oxide $\text{LaAlO}_3\text{-SrTiO}_3(001)$ heterostructures by incorporation of a strontium copper oxide nano-layer strongly reduces the impurity scattering, opening the door to high carrier mobility materials. This remote cuprate layer facilitates enhanced suppression of oxygen defects by reducing the kinetic barrier for oxygen surface exchange in the hetero-interfacial film system.

